**Supplementary Information**

# Dual Site Mo–$Mg_2Ni$ Catalyst Enhanced De/hydrogenation Kinetics in Magnesium with High Phase Stability

Kelin He[1,2], Yijian Chen[1,2], Jiang Liu[1,2], Haotian Guan[3], Jia Hu[1,2*], Qian Li[1,2*] and Yangfan Lu[1,2*]

[1]College of Materials Science and Engineering, National Engineering Research Center for Magnesium Alloys, National Key Laboratory of Advanced Casting Technologies, National Innovation Center for Industry-Education Integration of Energy Storage Technology, Chongqing University, Chongqing 400045, China

[2]Chongqing Institute of New Energy Storage Materials and Equipment, Chongqing 401135, China

[3]College of Materials Science and Engineering, Chongqing University of Technology, Chongqing 400054, China

**Corresponding authors**

*hujia827@cqu.edu.cn (J. Hu)

*cquliqian@cqu.edu.cn (Q. Li)

*yangfanlu@cqu.edu.cn (Y. Lu)

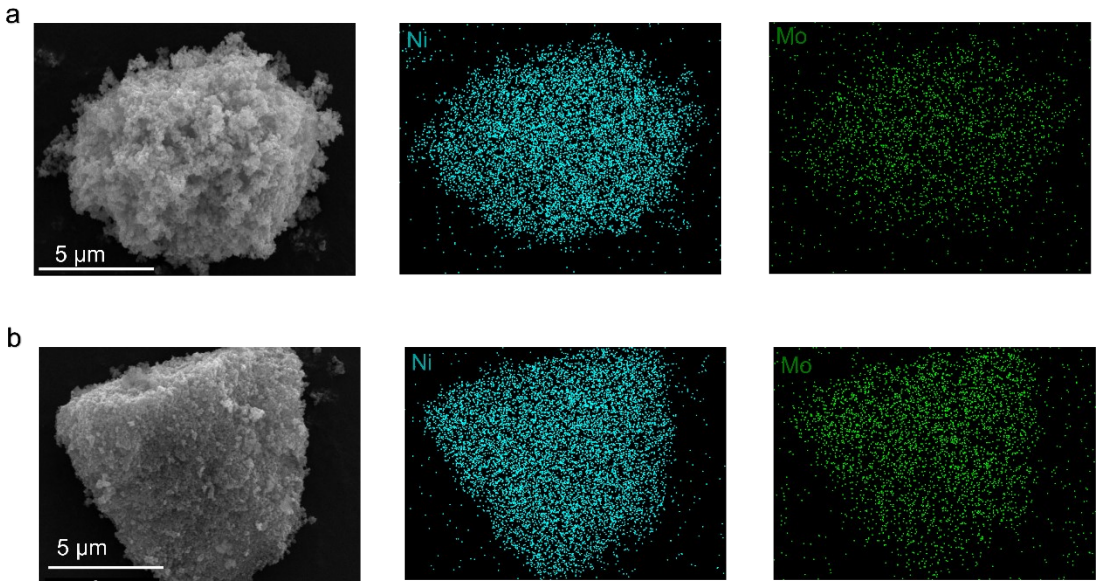


**Figure S1** SEM images and EDS mapping of a) $Mo_{0.1}Ni_{0.9}$ and b) $Mo_{0.2}Ni_{0.8}$.

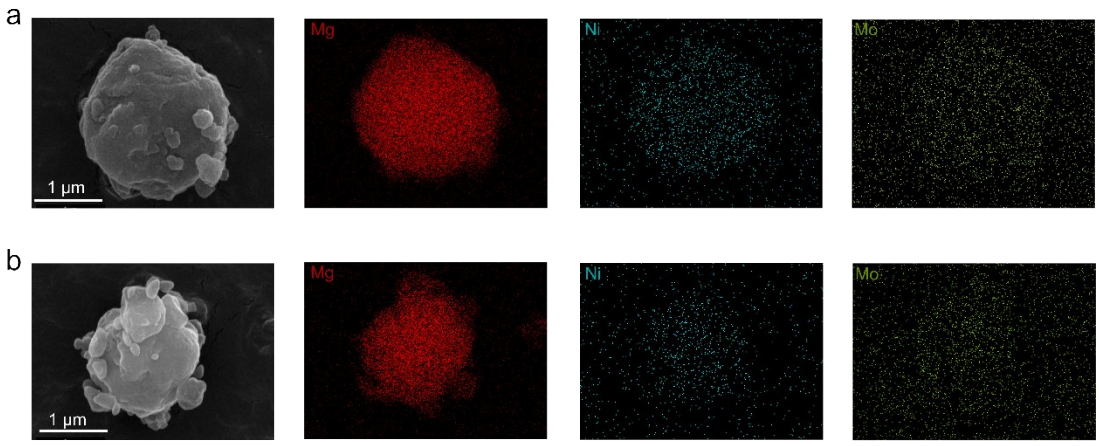


**Figure S2** SEM images and EDS mapping of a) $Mo_{0.1}Ni_{0.9}/MgH_2$ and b) $Mo_{0.2}Ni_{0.8}/MgH_2$ after ball-milling.

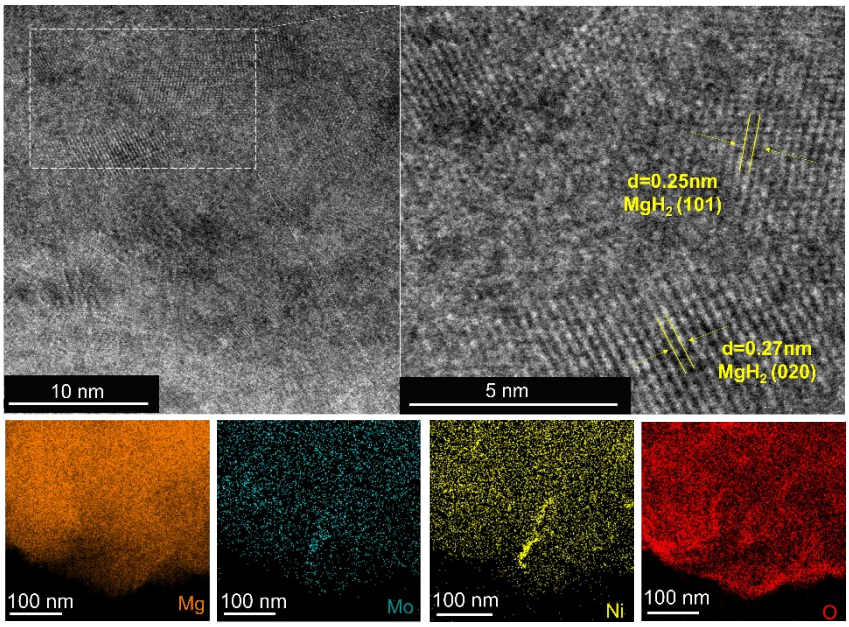


**Figure S3** TEM image for the ball-milled $Mo_{0.2}Ni_{0.8}/MgH_2$.

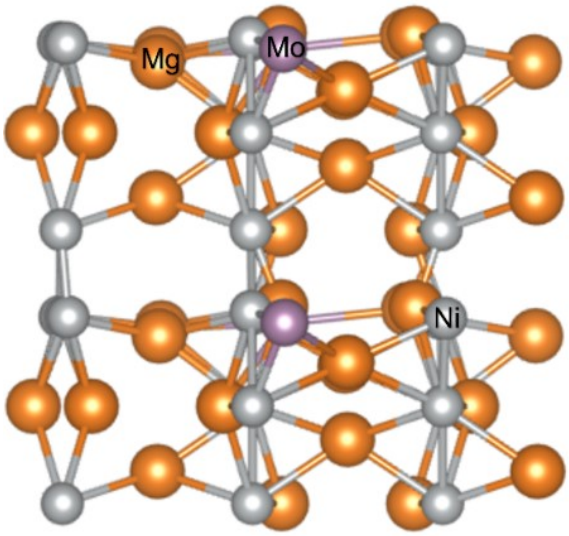


**Figure S4** The crystal structure of Mo-$Mg_2Ni$.

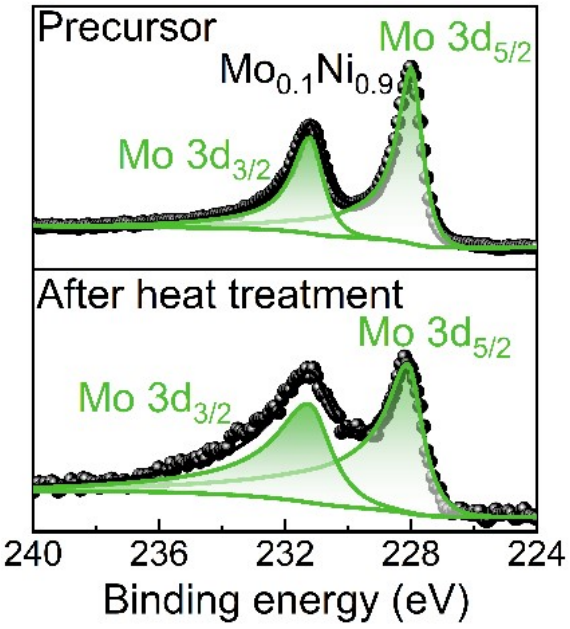


**Figure S5** Comparison of X-ray photoelectron spectroscopy (XPS) spectra for the $Mo_{0.1}Ni_{0.9}$ precursor and the heat treatment sample.

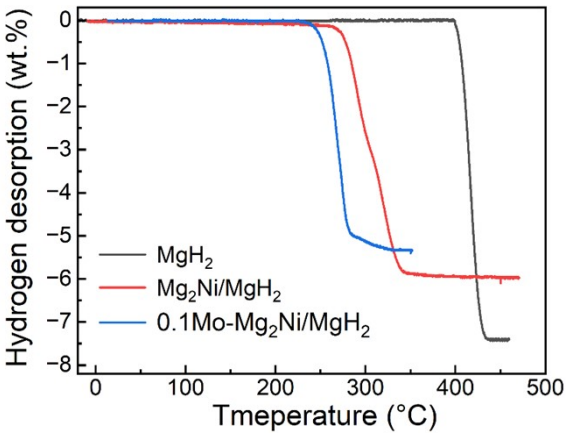


**Figure S6** TPD curves of $MgH_2$[1], $Mg_2Ni/MgH_2$[1] and $0.1Mo\text{-}Mg_2Ni/MgH_2$ after 50th cycles

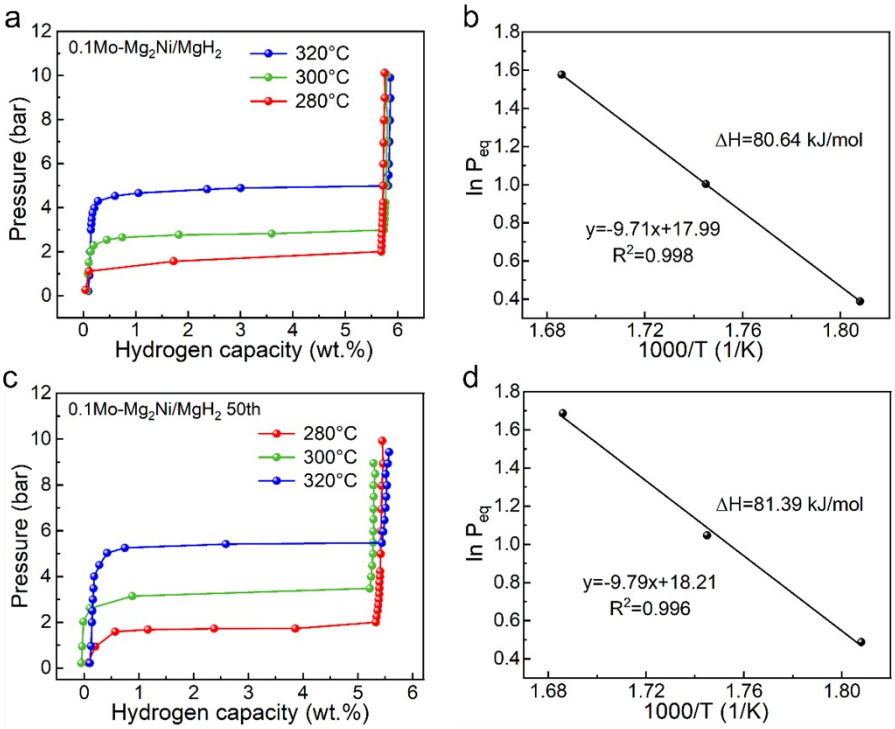


**Figure S7** (a) P–C–T curves of 0.1Mo-$Mg_2Ni$ /$MgH_2$ for hydrogen desorption at 280℃, 300℃ and 320℃. (b) Van't Hoff plots of 0.1Mo-$Mg_2Ni$ /$MgH_2$. (c) P–C–T curves of 0.1Mo-$Mg_2Ni$ /$MgH_2$ after 50 cycles for hydrogen desorption at 280℃, 300℃ and 320℃. (d) Van't Hoff plots of 0.1Mo-$Mg_2Ni$ /$MgH_2$ after 50 cycles.

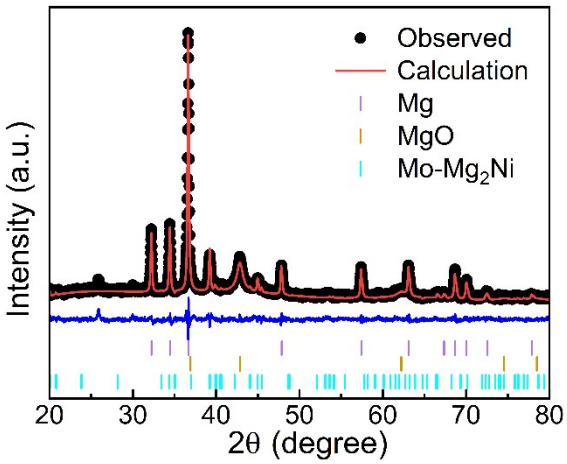


**Figure S8** XRD patterns of 30 wt%(0.1Mo-$Mg_2Ni$)/$MgH_2$ after 50 cycles

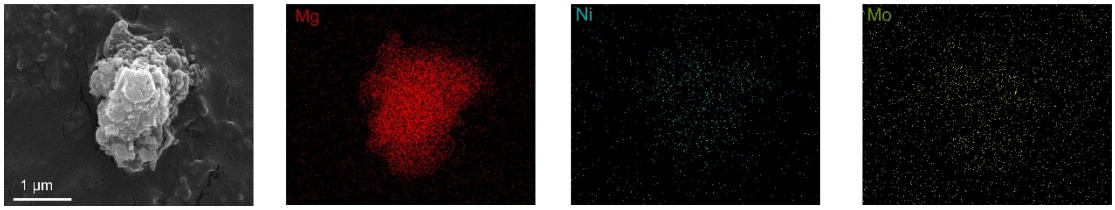


**Figure S9** SEM image and EDS mapping of 0.1Mo-$Mg_2Ni/MgH_2$ after 50 cycles.

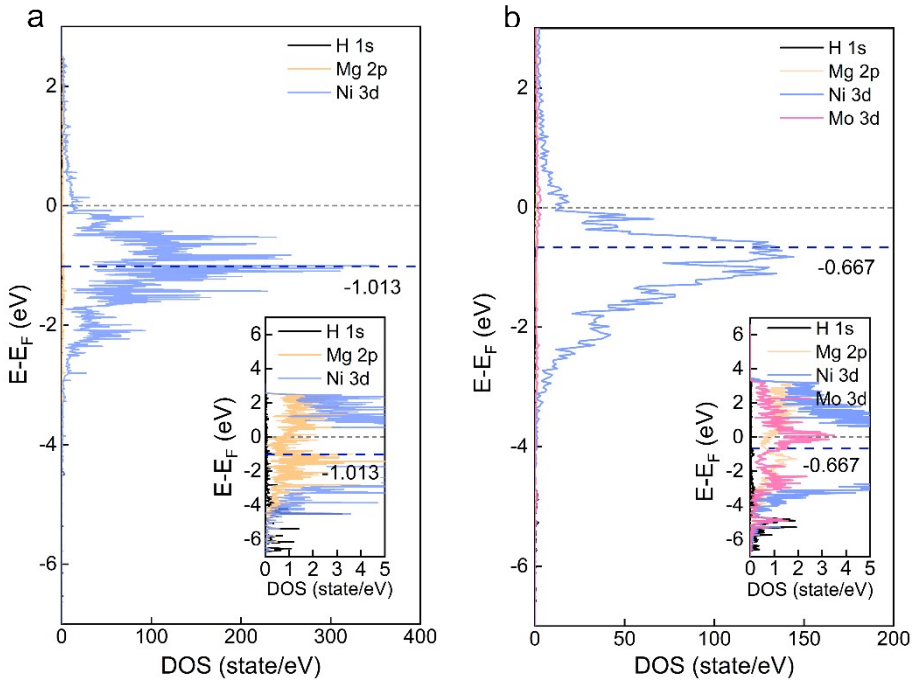


**Figure S10** (a) PDOS of Ni 3d, Mg 2p, and H 1s orbitals of $H_2$ adsorbed on $Mg_2Ni$. (b) PDOS of Ni 3d, Mg 2p, Mo 3d and H 1s orbitals of $H_2$ adsorbed on Mo-$Mg_2Ni$.

Table S1 TPD curves of different Ni-based catalysts with $MgH_2$ composites.

| Samples | T (°C) | Ref. |
|---|---|---|
| $MgH_2$+0.1Mo-$Mg_2Ni$ | 235 | This work |
| $MgH_2$+5wt.% $NiO/NiCo_2O_4$ | 241 | 2 |
| $MgH_2$+5wt.%Ni+5wt.%$ZrO_2$ | 255 | 3 |
| $MgH_2$+Ni@C@$CeO_2$ | 256 | 4 |
| $MgH_2$+5wt%$Ni_2P$ | 248 | 5 |
| Mg+5wt%NiS@$NTA_{0.107}$ | 281 | 6 |

Table S2 Dehydrogenation kinetics of different Ni-based catalysts with $MgH_2$ composites.

| Samples | Desorption kinetics | $E_a$(kJ/mol) | Refs |
|---|---|---|---|
| $MgH_2$+0.1Mo-$Mg_2Ni$ | 300℃, 5min, 6.04wt.% | 96.11 | This work |
| $MgH_2$ + 5 wt% FeNi/rGO | 300℃, 10min, 6.5wt.% | 93.6 | [7] |
| $MgH_2$−5wt.%Ni@CNT | 300℃, 16min, 3.7wt.% | 87.63 | [8] |
| $MgH_2$+10 wt% Ni/NiO | 300℃, 10min, 5.83wt.% | 87.21 | [9] |
| $MgH_2$+Ni/$Mo_2C$@C | 300℃, 20min, 6.35wt.% | 97.22 | [10] |
| $MgH_2$+$Ni_3ZnC_{0.7}$/Ni/ZnO | 300℃, 60min, 5.36wt.% | 93.06 | [11] |

Table S3 hkl-indexed diffraction peaks.

| Mg | $Mg_2Ni$ | $MgH_2$ | MgO |
|---|---|---|---|
| 32.181 (100) | 21.250 (100) | 27.912 (110) | 26.889 (111) |
| 34.397 (002) | 21.987 (101) | 35.732 (101) | 42.856 (200) |
| 36.615 (101) | 22.453 (004) | 39.885 (200) | 62.216 (220) |
| 47.816 (102) | 24.069 (102) | 41.098 (111) | 74.577 (311) |
| 57.376 (110) | 27.207 (103) | 44.833 (210) | 78.509 (222) |
| 63.067 (103) | 31.108 (104) | 54.614 (211) | |
| 67.325 (200) | 33.959 (006) | 57.679 (220) | |
| 68.638 (112) | 35.555 (105) | 61.334 (002) | |
| 70.014 (201) | 37.249 (110) | 65.271 (310) | |
| 72.508 (004) | 39.007 (112) | 66.135 (221) | |
| 77.840 (202) | 40.409 (106) | 68.693 (112) | |
| | 43.279 (200) | 69.732 (301) | |
| | 43.674 (201) | | |
| | 44.841 (202) | | |
| | 45.586 (107) | | |
| | 46.734 (203) | | |
| | 49.291 (204) | | |
| | 51.041 (108) | | |
| | 52.441 (205) | | |
| | 56.120 (206) | | |
| | 58.396 (210) | | |
| | 59.662 (212) | | |
| | 60.273 (207) | | |
| | 61.223 (213) | | |

| |
|---|
| 63.369 (214) |
| 64.862 (208) |
| 66.071 (215) |
| 67.166 (300) |
| 68.339 (302) |
| 69.300 (216) |
| 71.805 (304) |
| 73.029 (217) |
| 74.359 (305) |
| 77.438 (306) |
| 79.392 (220) |

Table S4 The Bader charge analysis of $H_2$ adsorbed $Mg_2Ni$

| | IN1 | INT1 | DIS1 | INT2 | DIF |
|---|---|---|---|---|---|
| H1 | 0.043 | 0.042 | 0.539 | 0.369 | 0.393 |
| H2 | -0.040 | -0.003 | 0.464 | 0.456 | 0.491 |
| Mg | -1.159 | -1.160 | -1.168 | -1.164 | -1.163 |
| Ni | 1.623 | 1.623 | 1.610 | 1.609 | 1.606 |

Table S5 The Bader charge analysis of $H_2$ adsorbed Mo-$Mg_2Ni$

| | IN1 | INT1 | DIS1 | INT2 | DIF |
|---|---|---|---|---|---|
| H1 | 0.026 | 0.026 | 0.357 | 0.444 | 0.412 |
| H2 | -0.023 | 0.009 | 0.383 | 0.369 | 0.360 |
| Mg | -1.178 | -1.178 | -1.181 | -1.174 | -1.179 |
| Ni | 1.548 | 1.552 | 1.546 | 1.547 | 1.537 |
| Mo | 0.820 | 0.735 | 0.592 | 0.355 | 0.701 |

# References

(1) Guan, H.; Liu, J.; Sun, X.; Lu, Y.; Wang, H.; Luo, Q.; Li, Q.; Pan, F. Titanium–Nickel Dual Active Sites Enabled Reversible Hydrogen Storage of Magnesium at 180 °C with Exceptional Cycle Stability (Adv. Mater. 26/2025). *Advanced Materials* **2025**, *37* (26), 2570178.

(2) Jiang, Y.; Si, N.; Wang, Z.; Zhang, H.; Jiang, W. Improved Hydrogen Storage Kinetic Properties of MgH2 with NiO/NiCo(Fe)$_2$O$_4$/(Ni). *Energy & Fuels* **2024**, *38* (24), 23804-23814.

(3) Tome, K. C.; Xi, S.; Fu, Y.; Lu, C.; Lu, N.; Guan, M.; Zhou, S.; Yu, H. Remarkable catalytic effect of Ni and $ZrO_2$ nanoparticles on the hydrogen sorption properties of $MgH_2$. *International Journal of Hydrogen Energy* **2022**, *47* (7), 4716-4724.

(4) Yu, Z.; Liu, X.; Liu, Y.; Li, Y.; Zhang, Z.; Chen, K.; Han, S. Synergetic catalysis of Ni@C@$CeO_2$ for driving ab/desorption of $MgH_2$ at moderate temperature. *Fuel* **2024**, *357*, 129726.

(5) Zhang, Q.; Zang, L.; Huang, Y.; Gao, P.; Jiao, L.; Yuan, H.; Wang, Y. Improved hydrogen storage properties of $MgH_2$ with Ni-based compounds. *International Journal of Hydrogen Energy* **2017**, *42* (38), 24247-24255.

(6) Xie, X.; Xiao, L.; Kimura, H.; Wu, P.; Du, W.; Wu, Y. Effects of layered walnut NiS@NTA on hydrogen storage performance of $MgH_2$. *Separation and Purification Technology* **2025**, *359*, 130837.

(7) Ji, L.; Zhang, L.; Yang, X.; Zhu, X.; Chen, L. The remarkably improved hydrogen storage performance of $MgH_2$ by the synergetic effect of an FeNi/rGO nanocomposite. *Dalton Transactions* **2020**, *49* (13), 4146-4154.

(8) Dai, Z.-y.; Zhang, B.; Kimura, H.; Xiao, L.-r.; Liu, R.-h.; Ni, C.; Hou, C.-x.; Sun, X.-q.; Zhang, Y.-p.; Yang, X.-y.; et al. Vermiform Ni@CNT derived from one-pot calcination of Ni-MOF precursor for improving hydrogen storage of $MgH_2$. *Transactions of Nonferrous Metals Society of China* **2024**, *34* (8), 2629-2644.

(9) Li, W.; Yang, X.; Hou, Q.; Lu, X.; Kong, J.; Su, J. Modification of $MgH_2$ hydrogen storage performance by nickel-based composite catalyst Ni/NiO. *Heliyon* **2024**, *10* (9).

(10) Yuan, Q.; Peng, C.; Yang, C.; Li, Y.; Zhang, Q.; Lv, Y.; Liu, G.; Liu, D. Facilitated hydrogen storage properties of MgH2 by Ni nanoparticles anchored on $Mo_2C$@C nanosheets. *International Journal of Hydrogen Energy* **2024**, *85*, 12-19.

(11) Dai, Z.-Y.; Wu, P.; Xiao, L.-R.; Kimura, H.; Hou, C.-X.; Sun, X.-Q.; Guo, S.-J.; Du, W.; Xie, X.-B. Non-stoichiometric $Ni_3ZnC_{0.7}$ carbide loading on melamine sponge-derived carbon for hydrogen storage performance improvement of $MgH_2$. *Rare Metals* **2024**, *44* (1), 515-530.